Interactions of relativistic electron-positron bunches with ambient plasmas in a regime relevant to the study of astrophysical jets

Contact *g.sarri@qub.ac.uk*

G. Sarri, J. R. Warwick, T. Dzelzainis, D. J. Corvan, M. Yeung, D. Doria, M. Zepf
Queen's University Belfast
University Road, Belfast BT7 1NN, UK

W. Schumaker
SLAC National Accelerator Laboratory
2575 Sand Hill Road, Menlo Park, California 94025, USA

L. Romagnani
Laboratoire LULI
Ecole Polytechnique, 91128, Palaiseau cedex. France

D. R. Symes
Central Laser Facility, STFC Rutherford Appleton Laboratory, Chilton, Didcot, OX11 0QX, UK

Introduction

Relativistic neutral electron-positron plasmas (EPPs) are an exotic state of matter, wherein the constituent matter-antimatter pair-particles are of equal mass, absolute charge, and density. EPPs are believed to be at the heart of multiple astrophysical phenomena, including Active Galactic Nuclei, Pulsars and the generation of ultra-bright and short-lived Gamma-Ray Bursts [1-4].

It is thought that the magnetospheres associated with compact, rotating astrophysical objects such as black holes and neutron stars are teeming with electron-positron plasmas produced via quantum electrodynamic cascades in the extreme fields near the surface of these objects. These astrophysical objects have been observed to produce outflows, and relativistic jets that generate non-thermal radiation spanning the electromagnetic spectrum from radio to gamma rays. The relativistic jets are observed to travel thousands of light years beyond the boundaries of their native galaxy, with very high collimation, and generally produce a termination shock due to their interaction with the intergalactic medium (IGM). It is thought that some of these astrophysical jets might be predominantly populated by relativistic electron-positron plasmas, and their interaction with the IGM has been proposed to be responsible for the generation of strong and long-lived magnetic fields, which ultimately play a central role in the generation of GRBs [5].

Due to their immense distance from Earth, it is virtually impossible to access the microphysics involved with these phenomena, and our knowledge of them must exclusively rely on the observation of their radiative signatures. Therefore, recreating these phenomena within laboratory conditions is imperative to testing the related theories, and advancing our understanding of such phenomena.

This report outlines an experiment, utilizing the Gemini laser system, which generated and propagated a relativistic neutral electron-positron plasma through an electron-ion plasma, in a regime pertinent to the study of astrophysical jets. Preliminary analysis of the results indicates strong beam filamentation, which in turn produces multi-Tesla magnetic fields. These fields, imaged via a proton radiography technique [6], are consistent with the generation mechanism thought to be at work at the termination shock of astrophysical jets.

Experimental Aims

The aim of the experiment was to characterize the dynamics of an ultra-relativistic electron-positron plasma propagating through a low-density background electron-ion plasma. The specific objectives were four-fold, and as follows:

1. Characterisation of the onset of transverse instability for a purely electronic beam, as a function of its Lorentz factor and density. This data would serve as a reference set for the subsequent points.
2. Study of filamentation pattern as electron-positron beam propagates in a background plasma as a function of the positron percentage in the beam, Lorentz factor and density of the background plasma.
3. Spectrally resolved study of filamentation for both an electronic and electron-positron beam.
4. Study of growth and persistence of electromagnetic fields in the background plasma using proton radiography.

Experimental Layout

The experiment was arranged as shown in Figure 1. The South beam of Gemini (duration of 40±5 fs and energy on target of ~12 J) was used to generate a relativistic electron beam using laser wake-field acceleration (LWFA). In order to achieve this, the beam was focused into a gas-cell using an F/20 parabola. An adaptive optic was used to remove aberrations resulting in a 30μm diameter spot. The focused intensity was then $\sim 2\times10^{19}$ Wcm^{-2}. The gas-cell was 10mm long and contained a gas mixture of 3% nitrogen and 97% helium. Optimum acceleration, in terms of maximum electron energy and charge was obtained for a background gas pressure of 500mb corresponding to an electron density of 4×10^{18} cm^{-3}. Shortly after exiting the gas-cell, the electron beam was incident on a lead converter. The converter itself was wedge-shaped and on a long travel vertical stage, allowing a continuous choice of the path-length of the electrons in the lead, ranging from 0 up to 40 mm. The second gas cell, used to hold the plasma with which the electron-positron beam was to interact, was placed immediately after the lead converter. It was critical to ensure a minimum path-length between the different components of the set-up as the temporal and spatial spread of the electron-positron beam would lead to a decrease in density below which the onset of filamentation would be expected to occur.

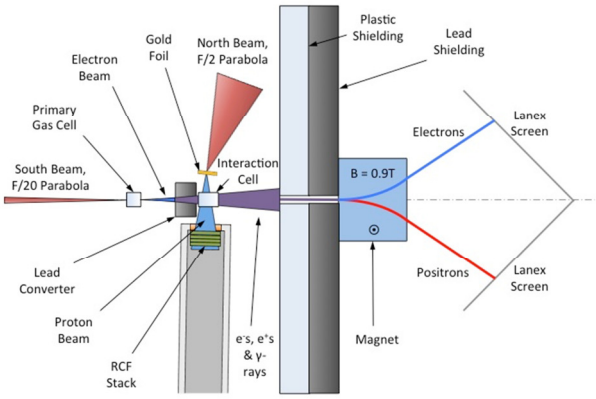

Figure 1. Schematic of the experimental layout. Outside of the experimental plane, and not shown in the figure, is a collection optic used to image the rear surface of the interaction cell to observe the beam profile

A magnetic spectrometer, using a 120 mm long, 0.9T magnetic field, was used to observe the spectra of the resulting electrons and positrons. This was shielded by 50mm thick lead and 50mm thick plastic. Lanex screens, observed with intensified CCDs (ANDOR iXon), were used as the recording medium. The screens and optical systems used to image the screens onto the CCDs were calibrated by placing image plates immediately before the screens for 3 consecutive shots. Image plate response to MeV electrons is well known and hence comparing CCD counts to PSL value can yield an absolute calibration of the diagnostic.

In order to observe the beam-profile after interaction with the plasma, the interaction gas-cell had, located on its rear, a position for an observation screen. This scintillation screen was tilted at 51.6° and imaged using an *f*/3 collection optic to a point near the chamber wall, and then re-imaged with a magnification of x20 onto a gated CCD (ANDOR iStar) which had a minimum gate time of ~1ns.

Finally, the North beam of Gemini was focused using an *f*/2 parabola onto a solid target positioned 7.5mm off the electron beam axis. This was used to generate a proton beam that could be used to perform proton radiography of the plasma after the electron-positron beam had passed, in order to observe the generation and dynamics of magnetic fields. These are predicted to occur from the interaction of the electron-positron beam and the background plasma, and should persist in the background plasma for many plasma periods (~1000 ω_p).

Results

The electron signal from the primary gas cell was optimized empirically by performing wide scans in parameter space. The variables that could be altered were the density of gas in the primary cell, the position of the cell relative to focus, and pulse characteristics (which could be altered using the DAZZLER used in GEMINI to compensate for higher-order phase terms introduced by the amplifier sections). Figure 2 shows 11 consecutive shots taken prior to a data run. The laser beam was apodised (~12cm, compared to a 15 cm full diameter beam) resulting in an energy on target of approximately 12J.

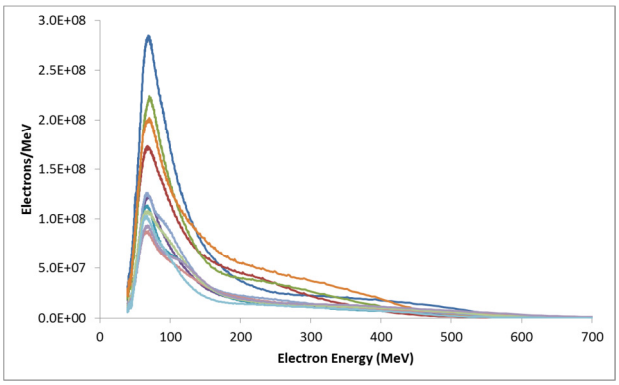

Figure 2. Electron spectra for 11 consecutive shots taken immediately prior to a data run

Once a satisfactory electron beam was obtained, the lead converter was inserted in its path. The neutrality of the beam was confirmed in a series of shots prior to data collection. Figure 3, comprises of 5 sample Lanex measurements, which show the evolution of the electron-positron spectra as the lead thickness is increased in multiples of the radiation length for lead (L_{rad} = 5.6mm). The generated lepton beam measures a positron population ratio of ~10% for a target thickness of $1L_{rad}$, (consistently with Ref. [7]) but the population grows to almost 50% at $5L_{rad}$ (consistently with Ref. [8]). Figure 4 shows the averaged populations of electrons and positrons as a function of converter thickness, which follows closely the behavior exhibited on previous experiment [8]. Neutrality is achieved after the primary electron beam has propagated through 2.5cm of lead (i.e. $5L_{rad}$).

It has been noted that the beam is non-neutral at lepton energies below ~5-10MeV [8]. This is due to the fact that pair production is caused by gammas released during the collision of an electron (or positron) with a lead atom, but at electron energies below 7.43MeV (7.16 MeV for positrons) the dominant energy loss mechanism is ionization of atomic electrons. This means that free electrons are produced in much greater numbers by the lower energy collisions. FLUKA simulations indicate that the resulting charge ratio across the whole spectral range is close to 55% electrons and 45% positrons. Simulations (as discussed in Ref. [8]) show that this charge imbalance has no perceivable effect on the interaction of the bunch with the background plasma.

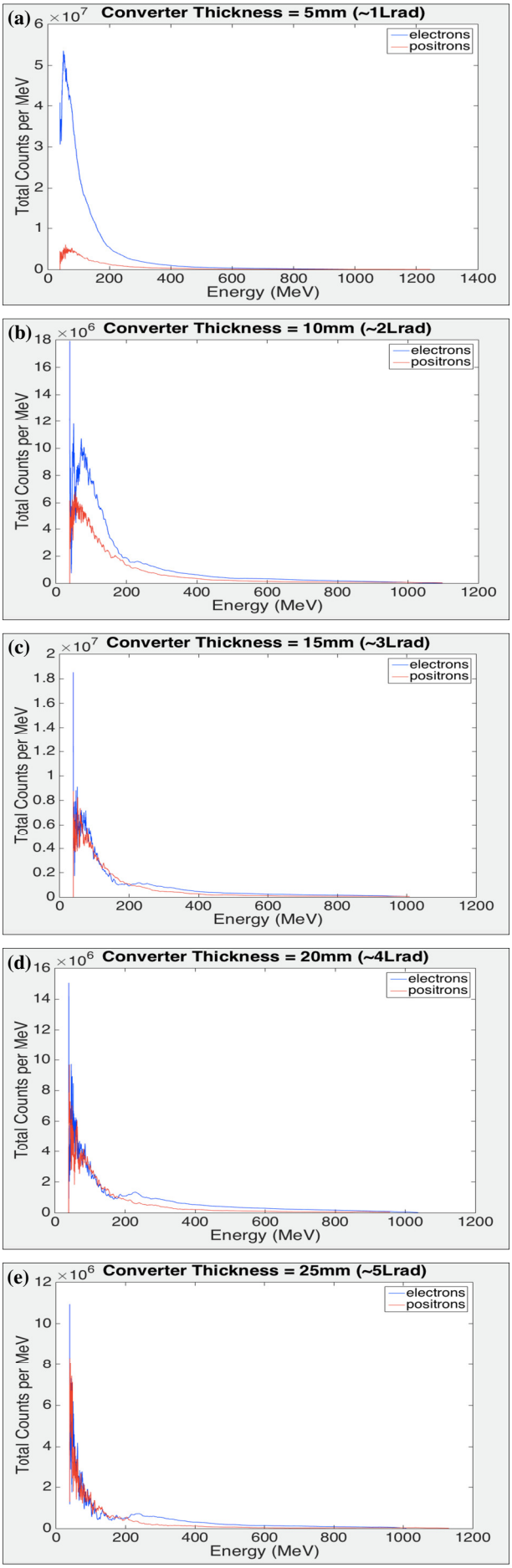

Figure 3. e^-/e^+ spectra generated from different lead converter thicknesses in steps of the radiation length with (a) 5mm, (b) 10mm, (c) 15mm, (d) 20mm, and (e) 25mm

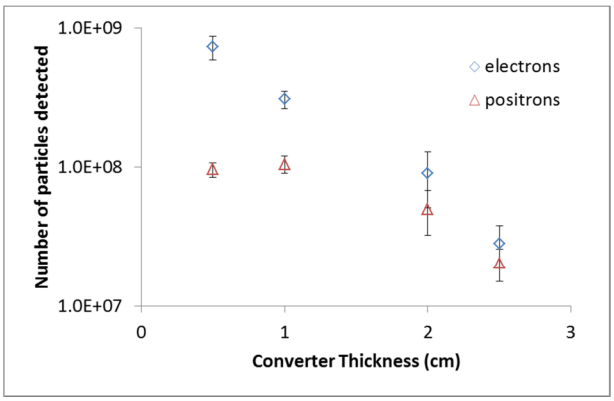

Figure 4. Numbers of electrons and positrons detected as a function of converter thickness. The beam asymptotically approaches neutral and can be seen to be near neutral at a converter thickness of 2.5cm

Preliminary analysis of the Radiochromic Film (RCF) garnered from proton radiography has been promising. The RCFs shown in Figure 5 (a) and (b) show the observable difference in the respective plasma dynamics of a pure electron beam and a neutral electron-plasma beam as they propagate through a 50mb plasma background. In both RCFs, the lepton beam is observed to travel through the background plasma from the right-hand side (RHS) of the RCF image to the left-hand side (LHS). The blank region on the RHS of 5(b) is the edge of the gas-cell wall.

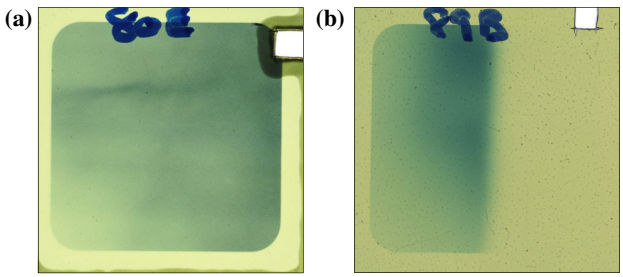

Figure 5. RCF taken from (a) a pure electron beam, and (b) a neutral electron-positron beam propagating through a background plasma contained within the interaction gas cell

For a pure electron beam propagating through an electron-ion plasma, the silhouette of a channel can be seen on the RCF in Figure 5(a). This channel is the result of the background plasma electrons being forced out of the path of the propagating electron beam. This leaves a positively charged channel (due to the population of comparatively slow reacting ions being left behind) within the background plasma, surrounded by a higher concentration of negative charge. The proton beam will therefore undergo a transverse deflection away from the positive channel, and towards the enveloping negatively charged region, which results in the higher proton concentration forming the observable outline of the channel. In contrast, a neutral electron-positron plasma beam does not form a channel in the background plasma, but instead undergoes filamentation beam instability, whereby the associated, and oppositely orientated magnetic fields of the constituent positively charged positrons, and negatively charged electrons, causes the electrons and positrons to bunch into same species filaments of positive and negative charge (as confirmed by Particle-In-Cell simulations, see Fig. 6 in Ref. [8]). These filaments of opposing currents give rise to regions of intense, opposing magnetic fields that act to push the filaments apart. Preliminary analysis indicates that the proton deflection pattern observed in Figure 5b arises from these magnetic fields being frozen in the background plasma. The blank area on the RHS is the gas-cell wall through which the e^-/e^+ beam enters, and it can be seen that

the protons are concentrated mainly in 2 lobes next to the wall in the early interaction stage. A region of lower concentration can be seen between the lobes, and this suggests that 2-3 filaments may have formed, with the proton beam being deflected according to the resultant intense magnetic fields. As the filaments diverge, the beam starts to lose the density necessary to maintain collective behaviour, and this would explain why the lobes only extend 1-2mm into the plasma, which is in stark contrast to the pure electron beam which can be seen to propagate the full width of the RCF.

Closer examination of the RCF in Figure 5(b) is shown in Figure 6(a). A lineout was taken transverse to the beam propagation direction (see dashed white line), and the proton densities (solid black line) and related magnetic fields (dashed green line) within the plasma were estimated and plotted (see Figure 6 (b)). It can be seen that a modulating magnetic field with peak strengths of approximately ±50T have been generated within the plasma, and this is in good agreement with PIC simulations [8].

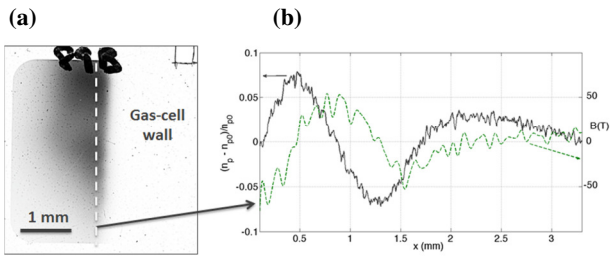

Figure 6. (a) RCF showing generation of magnetic fields in the background plasma as a result of filamentation of the neutral electron-positron beam; (b) A lineout shows how magnetic fields of approximately ±50T are generated transverse to the beam propagation direction.

Conclusions

A relativistic, neutral electron-positron plasma was successfully generated and propagated through an ambient electron-proton plasma. Preliminary analysis of the RCF suggests that beam filamentation of the neutral electron-positron plasma has been observed, with the generation of intense magnetic fields that are of strengths comparable to predictions made with PIC code simulations. The generation mechanism at work in the present experiment is qualitatively similar to what expected to occur at the termination shock of electron-positron astrophysical jets.

Acknowledgements

The authors are grateful for all the support provided by the staff of the Central Laser Facility. G. Sarri acknowledges support from EPSRC (grant No: EP/L013975/1).

References

1. R. D. Blandford and R. L. Znajek, Mon. Not. R. Astr. Soc. **179**, 433 (1977).
2. P. Goldreich and W. H. Julian, Astrophys. J. **157**, 869 (1969).
3. M. C. Begelman, D. Blandford and J. Rees, Rev. Mod. Phys. **56**, 255 (1984).
4. J. F. C. Wardle et al., Nature **395**, 457 (1998).
5. M. V. Medvedev and A. Loeb, Astrophys. J. **526**, 697 (1999).
6. G. Sarri et al. New J. Phys. **12** 045006 (2010).
7. G. Sarri et al. Phys. Rev. Lett. **110**, 255002 (2013).
8. G. Sarri et al. Nature Communications **6**, 6747 (2015).